Combustion and Flame 269 (2024) 113668

Contents lists available at ScienceDirect

Combustion and Flame

journal homepage: www.sciencedirect.com/journal/combustion-and-flame

Predicting extinction limits of concurrent smoldering spread by a reduced analytical model

Pichayaporn Viriya-amornkij [a], Kazunori Kuwana [a,*], Xinyan Huang [b]

[a] Department of Global Fire Science and Technology, Tokyo University of Science, Chiba, 278-8510, Japan
[b] Department of Building Environment and Energy Engineering, The Hong Kong Polytechnic University, 11 Hung Hom, Kowloon, Hong Kong

ARTICLE INFO

Keywords:
Smoldering
Extinction limits
Analytical model
Airflow velocity
Limiting oxygen concentration (LOC)

ABSTRACT

Smoldering is a flameless combustion mode occurring on the surface of charring fuels, such as wood and cigarettes. Although the smoldering process is slow and has a low temperature compared to flaming, it is easy to be initiated by a weak heat source and persists under poor oxygen conditions. Extensive work has been done for flame extinction to develop scaling models to predict the limiting oxygen concentration (LOC), but limited work is available for the smoldering extinction. This study develops a reduced analytical model to predict the extinction limits of smoldering. The model simultaneously solves smoldering propagation rate, surface temperature, and surface oxygen mass fraction as part of the solutions. The extinction limit is determined as the critical condition where solutions satisfying all governing equations cease to exist. The model provides a qualitative description and captures the essential characteristics of a previous experiment. The smoldering rate decreases with increasing fuel diameter, and a larger-diameter fuel is easier to extinguish. The mechanisms of the extinction process are investigated, showing the dominant role of radiative heat loss in the smothering limit at low airflow velocities and convective heat loss near the blowoff limit at high airflow velocities. Further analysis of the effect of oxygen concentration shows an increasing trend of LOC with fuel diameter, and the smothering branch cannot be predicted without considering the heat loss through radiation from the solid surface.

Novelty and Significance Statement: The novelty of this research is the prediction of smoldering propagation rates and extinction limits across various fuel diameters using a reduced analytical model. The model is modified to accommodate a thin fuel configuration and high airflow velocity condition, where convective heat and mass transfer play a more important role. The model's significance is that it not only provides essential insights into the mechanisms but also has the capability to simultaneously determine key parameters such as spread rate, reaction temperatures, and surface oxygen concentration as part of the solutions. Additionally, this study demonstrates the model's ability to reproduce the limit conditions, including smothering/blowoff limits and limiting oxygen concentration (LOC).

1. Introduction

The extinction of combustion processes is one of the most crucial topics related to fire safety. This complex phenomenon is influenced by various factors, including external air velocity [1–3], oxygen concentration [2,4], moisture content [5], sample size [6], and gravity level [7,8]. The flammability of a material is often characterized by its limiting oxygen concentration (LOC), which is the lowest oxygen concentration required to support the reaction. Over the past few decades, substantial research efforts have delved into understanding the limiting conditions for flaming spread over solid fuels in both normal and microgravity conditions. Fernandez-Pello et al. [2] conducted experiments on flame propagation over thick PMMA and thin paper sheets with varied oxygen concentrations and forced flow velocities. Osorio et al. [4] investigated the limiting conditions of flame spread for fire-resistant fabrics. They found a strong influence on oxygen concentration and radiant flux.

More recently, increased research attention has been directed towards fire safety in spacecraft. Olson et al. [7], Takahashi et al. [8], and Bhattacharjee et al. [9,10] explored the flame spread along a thin solid fuel in a microgravity environment. A flammability map is constructed based on the experimental data across a wide range of airflow velocities. Scaling analysis was employed to assess the flammability limits, using two non-dimensional parameters, i.e., the Damköhler number (the ratio

---

* Corresponding author.
E-mail address: kuwana@rs.tus.ac.jp (K. Kuwana).

https://doi.org/10.1016/j.combustflame.2024.113668
Received 22 April 2024; Received in revised form 13 August 2024; Accepted 13 August 2024

Nomenclature

a	strain rate [s^{-1}]
B_i	pre-exponential factor of reaction i [balance]
c	specific heat capacity [J/kg K]
d	fuel diameter [m]
D	mass diffusivity [m^2/s]
E_i	activation energy of reaction i [J/mol]
h	heat transfer coefficient [W/m^2 K]
h_m	mass transfer coefficient [m/s]
Q_i	heat of reaction i [J/kg]
R	universal gas constant [J/mol K]
T	temperature [K]
u_a	forced airflow velocity [m/s]
u_g	gas velocity [m/s]
v_P	pyrolysis-gases velocity [m/s]
v_{sm}	smoldering propagation rate [m/s]
x	moving coordinate [m]
Y	mass fraction [–]
Greek symbols	
α	thermal diffusivity [m^2/s]
ε	emissivity [–]
ϕ	volume fraction [–]
λ	thermal conductivity [W/m K]
μ	viscosity [Pa s]
$\nu_{i,j}$	mass-based stoichiometric coefficients of species j in reaction i [kg/kg]
ρ	density [kg/m^3]
σ	Stefan-Boltzmann constant [W/m^2 K^4]
$\dot{\omega}_i''$	rate of reaction i [kg/m^2 s]
Subscripts	
0	initial value
C	char
F	fuel
g	gas phase
O	oxygen
P	pyrolysis products
p	pyrolysis front
s	surface

of the residence time to chemical reaction time) and a radiative loss parameter. The flame spread is suppressed due to the finite kinetic effect and heat-loss mechanisms. These limits were determined by calculating the conditions where the sum of the radiative loss and the reciprocal of the Damköhler number equals unity. The LOC of a thin cellulose fuel was identified to be around 15% at 4–6 cm/s flow velocities.

Compared to flaming spread, the smoldering process is more easily initiated by a weaker heat source and can be sustained in extreme conditions, such as high airflow velocity and poor oxygen supply [11]. Moallemi et al. [12] performed smoldering experiments and numerical simulations at different oxygen mass fractions. The LOC of a wood-charcoal sample was found at 13.5% at an inlet gas flow rate of 0.3 mm^3/s. Richter et al. [13] examined the ignition and burning behavior of a particleboard experimentally and computationally. Their results indicated that the particleboard undergoes the smoldering reaction within the oxygen concentration range from 4 to 15% at a heat flux of 30 kW/m^2. Despite some earlier works concentrating on determining the LOC of the smoldering process, there seems to be a gap between available experimental data and an insufficient theoretical understanding of the oxygen supply thresholds.

So far, the models proposed to predict the LOC [8,14,15] have been discussed based on scaling analysis, considering simplified heat balance around the solid preheated zone. These phenomenological arguments can only predict the limiting condition of extinction by assuming a balance between heat generation and heat loss. However, a deep systematic understanding of the mechanisms driving the extinction phenomena cannot be provided. Therefore, the present study aims to develop a more rigorous model to investigate the extinction mechanisms at various airflow velocities and oxygen concentrations. The steady, one-dimensional smoldering model, initially proposed by Kadowaki et al. [16], is modified to predict the smothering and blowoff limits of a smoldering process for various thickness samples. Unknown parameters, such as smoldering rate, surface oxygen concentration, pyrolysis temperature, and char-oxidation temperature, are determined simultaneously as part of the solutions. The model is validated with a previous experiment by Lin et al. [1], in which an incense stick of 1.5, 2.5, or 5 mm in diameter was burned in a forced airflow. Subsequently, the model is further applied to predict the critical airflow velocity and the LOC.

2. Mathematical model

2.1. Model description

A steady, one-dimensional model of forward smoldering, previously proposed by Kadowaki et al. [16], is modified to accommodate a thin fuel configuration (Fig. 1) tested in [1]. The following assumptions are made to simplify the equations:

1) Steady smoldering is assumed in a moving coordinate system fixed at the fuel surface ($x = 0$), as shown in Fig. 1. The following two reactions of pyrolysis and char-oxidation are considered to model the smoldering process.

$$\mathrm{F} \rightarrow \nu_{1,C}\,\mathrm{C} + \nu_{1,P}\,\mathrm{P} \tag{R1}$$

$$\mathrm{C} + \nu_{2,O}\,\mathrm{O} \rightarrow (1 + \nu_{2,O})\mathrm{CO/CO_2} \tag{R2}$$

Both reactions are assumed to take place only at the interface: pyrolysis front ($x = x_p$) and char-oxidation front ($x = 0$), respectively. This assumption is reasonable because the chemical reaction rate is much faster than the diffusion rate. The comparison between the reaction and oxygen diffusion rates leads to the following dimensionless quantity: $\pi = [d\nu_{2,O}B_2\rho_C\phi_C\exp(-E_2/RT_s)]/D_O$, a similar dimensionless parameter to the Thiele modulus. With the representative value of $T_s = 1200$ K, the following results are obtained: $\pi = 71$ for $d = 1.5$ mm, and $\pi = 235$ for $d = 5$ mm. Its high value makes the surface oxygen concentration much lower than the ambient value. On the other hand, smaller diameters may lead to a reaction-limited regime, necessitating a new modeling approach.

The fresh fuel is steadily consumed at a constant velocity v_{sm} by pyrolysis reaction (R1) at $x = x_p$ to produce the char and pyrolysis gases. Then, the char reacts with oxygen through the char-oxidation reaction (R2) at $x = 0$ to produce the gas species moving along with the pyrolysis products into the gas phase at velocity $u_{g,s}$. The rates of pyrolysis and char-oxidation reactions are assumed to be first order in each reactant and are expressed in the following forms:

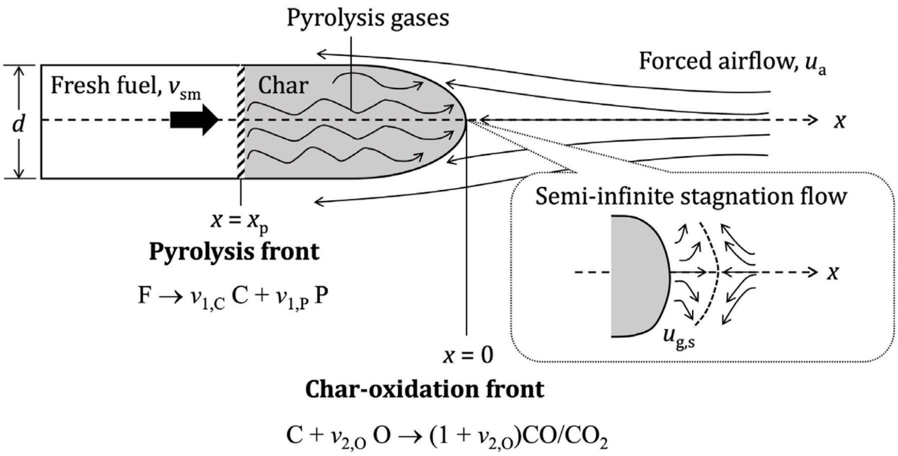

Fig. 1. Schematic diagram of the one-dimensional smoldering model.

$$\dot{\omega}_1'' = B_1 \rho_F \phi_F \exp\left(-\frac{E_1}{RT_p}\right) \tag{1}$$

$$\dot{\omega}_2'' = B_2 \rho_C \phi_C \rho_g Y_{O,s} \exp\left(-\frac{E_2}{RT_s}\right) \tag{2}$$

The bulk density of fuel and char are expressed as $\rho_F\phi_F$ and $\rho_C\phi_C$, respectively, where ϕ is the volume fraction.

2) The near-tip flow is modeled as a potential counterflow, following studies on counterflow diffusion flames of Tsuji-Yamaoka configurations [17], which have been modeled as a semi-infinite stagnation flow. The gas flow along the x direction, u_g, is hence modeled by Eq. (3), enabling one-dimensional treatment.

$$u_g = u_{g,s} - ax \tag{3}$$

where $u_{g,s}$ is the gas velocity at the fuel surface. Here, the velocity v_{sm} of the moving coordinate is neglected as $u_{g,s} >> v_{sm}$. The potential flow is characterized by the strain rate a, which dimensional consideration suggests is proportional to the forced airflow velocity, u_a, divided by the sample diameter, d. While Kadowaki et al. [16] considered a thick fuel, for which the assumption of semi-infinite stagnation flow is reasonable, the diameter of incense sticks used in [1] was as small as 1.5 mm. Therefore, convective heat loss and oxygen transfer at the tip are considered in this study using heat-transfer and mass-transfer coefficients to compensate for the multi-dimensional effect. Besides, the airflow velocity in [1] was much faster than [16] to achieve the blowoff conditions, making convective heat and mass transfer significant.

3) All material properties, including the gas density, are assumed to be constant.

2.2. Conservation equations

2.2.1. Mass balance equations

The mass balance in the solid phase is shown in Eqs. (4)–(6).

$$\rho_F \phi_F v_{sm} = \dot{\omega}_1'' \tag{4}$$

$$\nu_{1,C} \dot{\omega}_1'' = \dot{\omega}_2'' \tag{5}$$

$$\rho_F \phi_F v_{sm} = \rho_g u_{g,s} \tag{6}$$

Eq. (4) expresses the consumption of fresh fuel by pyrolysis reaction (R1). Eq. (5) indicates the steady-state condition; all char produced by reaction (R1) is consumed by char-oxidation reaction (R2). Eq. (6) corresponds to the overall mass balance; the fuel is entirely converted into gases.

2.2.2. Energy balance equations

The heat balance equations within the fresh fuel ($x < x_p$), char layer ($x_p < x < 0$), and gas phase ($x > 0$) are shown in Eqs. (7)–(9), respectively.

$$\rho_F \phi_F c_F v_{sm} \frac{dT}{dx} = \lambda_F \frac{d^2T}{dx^2} \tag{7}$$

$$\left[\rho_C \phi_C c_C v_{sm} + \rho_P (1 - \phi_C) c_P v_P\right] \frac{dT}{dx} = \lambda_C \frac{d^2T}{dx^2} \tag{8}$$

$$u_g \frac{dT}{dx} = \alpha_g \frac{d^2T}{dx^2} \tag{9}$$

The interface conditions at pyrolysis front ($x = x_p$) and char-oxidation front ($x = 0$) are described based on heat balance concepts, as shown in Eqs. (10) and (11), respectively.

$$\rho_F \phi_F c_F v_{sm} T_p - \lambda_F \left.\frac{dT}{dx}\right|_{x_{p^-}} + Q_1 \dot{\omega}_1'' = \left[\rho_C \phi_C c_C v_{sm} + \rho_P (1 - \phi_C) c_P v_P\right] T_p - \lambda_C \left.\frac{dT}{dx}\right|_{x_{p^+}} \tag{10}$$

$$\left[\rho_C \phi_C c_C v_{sm} + \rho_P (1 - \phi_C) c_P v_P\right] T_s - \lambda_C \left.\frac{dT}{dx}\right|_{0^-} + Q_2 \dot{\omega}_2'' - \sigma\varepsilon\left(T_s^4 - T_0^4\right) - h(T_s - T_0) = \rho_g c_g u_{g,s} T_s - \lambda_g \left.\frac{dT}{dx}\right|_{0^+} \tag{11}$$

Solving Eqs. (7)–(9) yields the temperature gradients needed to evaluate the interface conditions. Eq. (7) is solved with the boundary conditions of $T \rightarrow T_0$ as $x \rightarrow -\infty$ and $T = T_p$ at $x = x_p$, giving the temperature gradient, as shown in Eq. (12). Similarly, Eq. (8) with boundary conditions of $T = T_p$ at $x = x_p$ and $T = T_s$ at $x = 0$ leads to Eq. (13). Also, Eq. (9) with boundary conditions of $T = T_s$ at $x = 0$ and $T \rightarrow T_0$ as $x \rightarrow \infty$ leads to Eq. (14).

$$\left.\frac{dT}{dx}\right|_{x_{p^-}} = \frac{\rho_F \phi_F c_F v_{sm} \left(T_p - T_0\right)}{\lambda_F} \tag{12}$$

$$\lambda_C \left(\left.\frac{dT}{dx}\right|_{0^-} - \left.\frac{dT}{dx}\right|_{x_{p^+}}\right) = \left[\rho_C \phi_C c_C v_{sm} + \rho_P (1 - \phi_C) c_P v_P\right] \left(T_s - T_p\right) \tag{13}$$

$$\left.\frac{\mathrm{d}T}{\mathrm{d}x}\right|_{0^+} = (T_0 - T_s) \times \frac{\sqrt{2a/\pi\alpha_g}}{\mathrm{erfc}\left(\frac{-u_{g,s}}{\sqrt{2a\alpha_g}}\right)} \exp\left(-\frac{u_{g,s}^2}{2a\alpha_g}\right) \tag{14}$$

By substituting Eqs. (12) and (13) into Eq. (10), Eq. (15) can be obtained as follows.

$$\rho_F\phi_F c_F v_{sm} T_0 + Q_1\dot{\omega}_1'' = [\rho_C\phi_C c_C v_{sm} + \rho_P(1-\phi_C)c_P v_P]T_s - \lambda_C \left.\frac{\mathrm{d}T}{\mathrm{d}x}\right|_{0^-} \tag{15}$$

The total energy balance equation in the solid phase, Eq. (16), is derived by substituting Eq. (15) into Eq. (11). It includes terms representing the heat of reactions, the sensible heat of the fresh fuel and the gas, heat transfer due to gas-phase conduction, and heat loss by radiation and convection into the gas phase. Note that the value of x_p can be obtained by solving Eq. (8) in the char layer between x_p and 0 with the aid of Eqs. (10) and (12), given that the material properties of char and pyrolysis gases are known. Meanwhile, the value of v_P can be known by considering the mass balance across the pyrolysis front: $\rho_F\phi_F v_{sm} = \rho_C\phi_C v_{sm} + \rho_P(1-\phi_C)v_P$. Nevertheless, this study does not determine their values because they are not included in the total energy balance Eq. (16).

$$\begin{aligned} Q_1\dot{\omega}_1'' + Q_2\dot{\omega}_2'' + \rho_F\phi_F c_F v_{sm} T_0 - \rho_g c_g u_{g,s} T_s + \lambda_g \left.\frac{\mathrm{d}T}{\mathrm{d}x}\right|_{0^+} \\ - \sigma\varepsilon\left(T_s^4 - T_0^4\right) - h(T_s - T_0) = 0 \end{aligned} \tag{16}$$

The gas-phase heat conduction term in Eq. (16) can be evaluated using Eq. (14). The heat transfer coefficient is modeled as a function of the Reynolds number (Re). The following correlation for the airflow past single spheres proposed by McAdams [18] is applied in this study. The Re number can be calculated as $\mathrm{Re} = \rho_g u_a d/\mu_g$ with $\mu_g = \mathrm{Pr}\rho_g\alpha_g$, where $\mathrm{Pr} = 0.71$ is the Prandt number of the air.

$$\mathrm{Nu} = \frac{hd}{\lambda_g} = 0.31\mathrm{Re}^{0.6} \tag{17}$$

2.2.3. Oxygen balance equation

The oxygen balance can be expressed as Eq. (18), illustrating the balance between oxygen consumed at the surface and oxygen loss due to gas flow, oxygen diffusion caused by the concentration gradient, and convective oxygen supply by the forced airflow. Note that the unity Lewis number ($\mathrm{Le} = \lambda_g/\rho_g c_g D_O = \alpha_g/D_O = 1$) is assumed for simplicity. The oxygen concentration gradient appearing in Eq. (18) can be derived similarly to Eq. (14) by solving the oxygen balance equation in the gas phase, with the boundary conditions of $Y_O = Y_{O,s}$ at $x = 0$ and $Y_O \to Y_{O,0}$ as $x \to \infty$.

$$\nu_{2,O}\dot{\omega}_2'' + \rho_g u_{g,s} Y_{O,s} - \rho_g\alpha_g \left.\frac{\mathrm{d}Y_O}{\mathrm{d}x}\right|_{0^+} - \rho_g h_m\left(Y_{O,0} - Y_{O,s}\right) = 0 \tag{18}$$

The convective oxygen mass transfer is also included in the oxygen-balance equation. Brian et al. [19] presented mass transfer coefficients for spheres suspended in an agitated liquid, expressing the Sherwood number (Sh) as a function of the Reynolds (Re) and Schmidt (Sc) numbers, as in Eq. (19). The Sc number can be calculated as $\mathrm{Sc} = \mu_g/\rho_g D_O$.

$$\mathrm{Sh} = \frac{h_m d}{D_O} = \left[4 + 1.21(\mathrm{ReSc})^{0.67}\right]^{0.5} \tag{19}$$

The five governing equations for mass, energy, and oxygen balance, Eqs. (4)–(6), (16), and (18), are employed to solve the following five unknown parameters: $u_{g,s}$, T_p, T_s, v_{sm}, and $Y_{O,s}$, utilizing the non-linear regression method available in the Solver Add-In of Microsoft Excel. The input parameters are listed in Table 1. The sensitivity analysis of B_2, ε, and E_2 is conducted, and the results are presented in Appendix A.

Table 1
Model input parameters.

Parameters	Value	Unit	Ref.
$\nu_{1,C}$	0.24	kg/kg	[20]
$\nu_{1,P}$	0.76	kg/kg	[20]
$\nu_{2,O}$	1.65	kg/kg	[20]
B_1	2×10^5	m/s	[16]
E_1	120	kJ/mol	[16]
Q_1	−570	kJ/kg	[16]
B_2	1.8×10^3	m^4/kg s	This study [a]
E_2	120	kJ/mol	[16]
Q_2	2.16×10^4	kJ/kg	[16]
$\rho_F\phi_F$	720	kg/m^3	[1]
c_F	1400	J/kg K	[16]
c_g	1140	J/kg K	[16]
ρ_g	0.35	kg/m^3	This study [b]
λ_g	0.026	W/m K	[21]
ε	0.4	–	This study [a]
σ	5.67×10^{-8}	$W/m^2 K^4$	[22]
R	8.314×10^{-3}	kJ/mol K	[22]
T_0	298.15	K	–

[a] Estimated using the experimental data in [1].

[b] Air density at 1000 K.

3. Results and discussion

In this section, the predicted results from the model concerning the limit conditions are first introduced. These results are then validated against the experimental data [1]. Furthermore, additional discussions are provided on the fundamental mechanisms of extinction and the LOC.

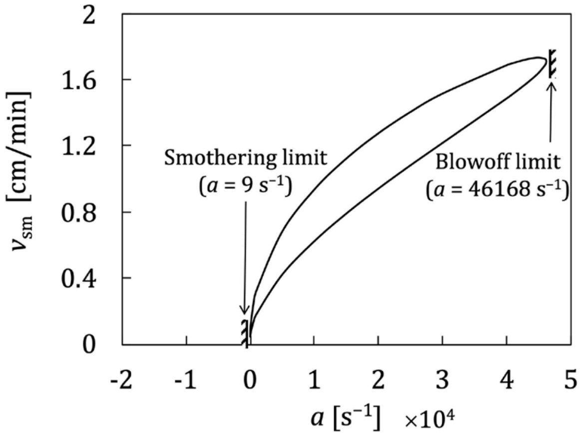

Fig. 2. Predicted smoldering rate, v_{sm}, as a function of strain rate a for $d = 5$ mm.

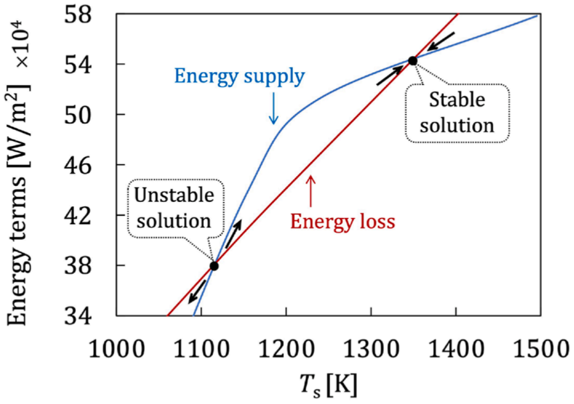

Fig. 3. Stability of the lower and upper solutions based on energy balance concept at $a = 10^4$ s^{-1}.

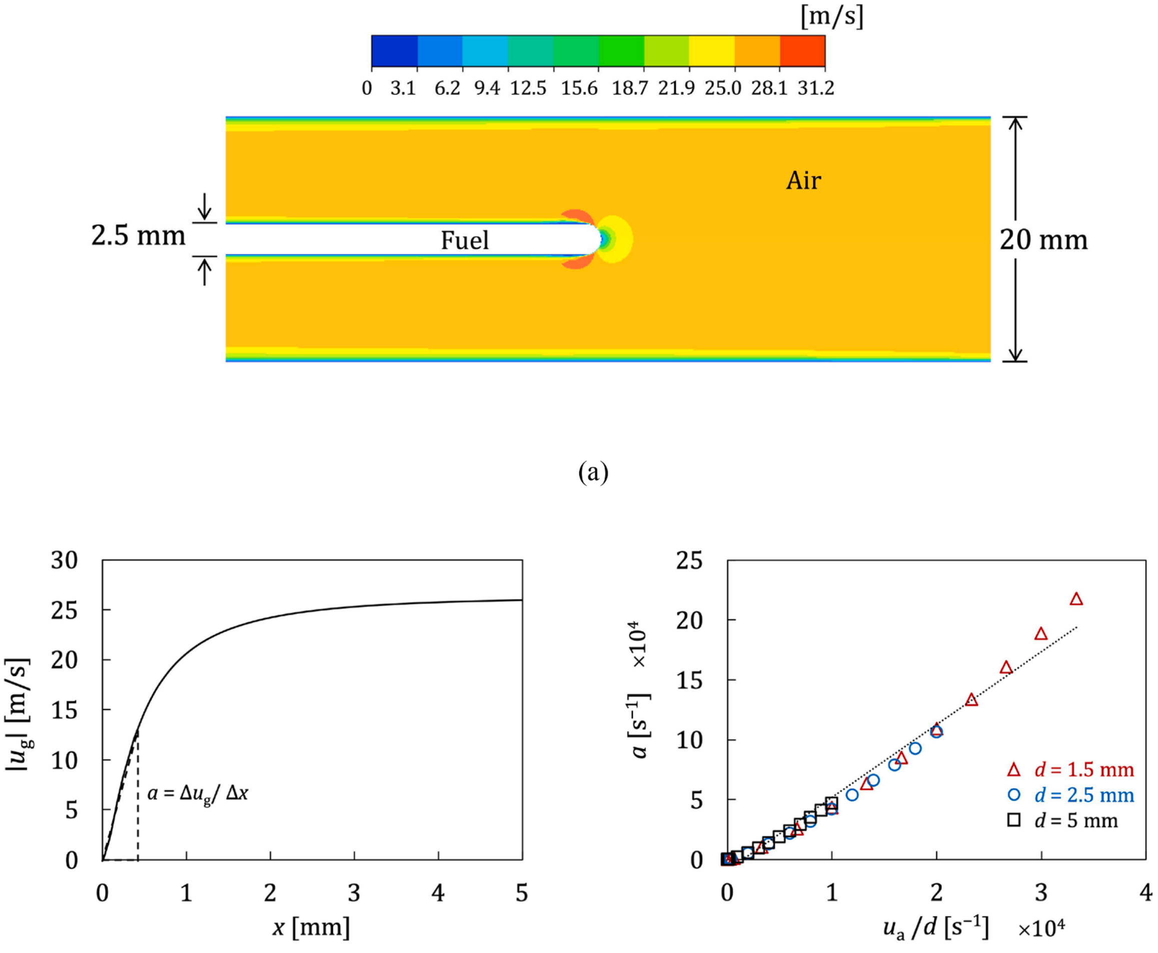

(a)

(b)

(c)

Fig. 4. 2-D flow simulation: (a) velocity contour for $d = 2.5$ mm at $u_a = 25$ m/s, (b) centerline velocity to obtain near-tip strain rate, and (c) correlation between u_a and a for various diameters. Red, blue, and black: $d = 1.5$, 2.5, and 5 mm.

3.1. *Smoldering limit conditions*

The obtained results of smoldering propagation rates for $d = 5$ mm are selected as a representative example of the predictions, as shown in Fig. 2. The model successfully predicts two extinction conditions: smothering at a low strain rate and blowoff at a high strain rate. Each extinction limit is identified as a turning point, where the solutions satisfying all the governing equations cease to exist beyond it. Between the two limits, two solutions exist, i.e., the upper and lower branches. However, the lower branch is disregarded because it is unstable and lacks physical meaning. Fig. 3 illustrates the stability of solutions at $a = 10^4$ s^{-1} by plotting the first three terms (energy supply) and the rest (energy loss) of Eq. (16) as a function of the surface temperature, T_s. There are two steady-state solutions where the energy supply and loss terms are balanced. The upper solution is stable because energy loss exceeds energy supply when T_s increases, while the situation is opposite when T_s decreases. Therefore, T_s can return to the steady-state solution under a small perturbation. A similar consideration also indicates the unstable nature of the lower solution. The upper branch in Fig. 2 demonstrates an increasing trend in the smoldering rate with a slight decrease near the blowoff limit. Further discussion will be given later in Section 3.3.

3.2. *Strain rate estimation*

To validate the model with the experiment, the relationship between strain rate a and forced airflow velocity u_a must be established because the former is used in the present model as a flow parameter, whereas the latter is the experimental parameter. For this purpose, ANSYS Fluent was employed. An axisymmetric 2-D computational domain, consistent with the experimental setup of Lin et al. [1], where the diameter of the outer tube is 20 mm, was adopted. The distance between the inlet boundary condition and the fuel tip was fixed at a representative experimental value of 5 cm. The forced airflow velocity was varied up to 50 m/s for three different fuel diameters, $d = 1.5$, 2.5, and 5 mm. No chemical reactions were included, and the tip (the hemisphere surface) temperature was fixed at a representative smoldering temperature of 1000 K. The temperature of the outer tube's walls was fixed at an ambient temperature of 300 K. The side boundary of the fuel was coupled with the heat conduction equation within the fuel. The temperature-dependent air properties were used.

While the k-ω turbulence model was used, laminar calculations were attempted for small Reynolds-number cases; the results were nearly identical regarding the obtained correlation between the strain rate and the forced airflow velocity. The computational cell size is 0.1 mm, which was confirmed to be fine enough to eliminate the grid-size dependence.

Fig. 4(a) shows the steady-state near-tip velocity distribution obtained for $u_a = 25$ m/s, which yields the centerline velocity profile shown in Fig. 4(b). The slope of the curve near the fuel surface gives the strain rate a. As shown in Fig. 4(c), a nearly linear, universal correlation, Eq. (20), is obtained between a and u_a/d for the different fuel diameters. The correlation is used to convert the experimental parameter u_a to the model parameter a.

$$a = 5.57\left(\frac{u_a}{d}\right) \tag{20}$$

3.3. *Model validation*

The robustness of the model in predicting experimental results in [1] is tested. Fig. 5(a) compares the predicted smoldering rate with the experimental data. The model correctly reproduces the experimental trends: the smoldering rate and the blowoff strain rate decrease with an increase in fuel diameter. Considering the model's simplicity, its accuracy in predicting the smoldering rate and the blowoff limit is reasonable. Good agreement between experimental and predicted blowoff strain rate is found for thin diameter ($d = 1.5$ mm), with less than 5% error, yielding $a = 1.72 \times 10^5$ s^{-1} and 1.66×10^5 s^{-1} for experiment and prediction, respectively. On the other hand, higher errors are observed in thicker diameters, giving $a = 2.75 \times 10^4$ s^{-1} for the experiment and $a = 4.62 \times 10^4$ s^{-1} for the prediction of the 5 mm fuel.

The consequences of our model being derived based on one-dimensional conservation concepts are discussed here. Firstly, the effects of fuel diameter are incorporated only through the heat (h) and mass (h_m) transfer coefficients in the present model. As a result, the dependence of the smoldering rate and extinction limits is solely controlled by the Nusselt-Reynolds and Sherwood-Reynolds correlations. Analysis shows that the Nusselt-Reynolds correlation has a crucial impact on the dependence of the blowoff limit on diameter (see Appendix B for more details). On the other hand, the critical strain rate for smothering extinction is significantly overpredicted without considering convective mass transfer. Both correlations are obtained for single spheres in forced flows, which differ from the present configuration and could contribute to errors in this study. While using heat and mass transfer coefficients allows the present simple analysis, it also poses a limitation of the model. Secondly, achieving uniform conditions, i.e., uniform temperature and uniform oxygen concentration at the reaction front, is challenging for thick fuels, causing high error predictions in $d =$

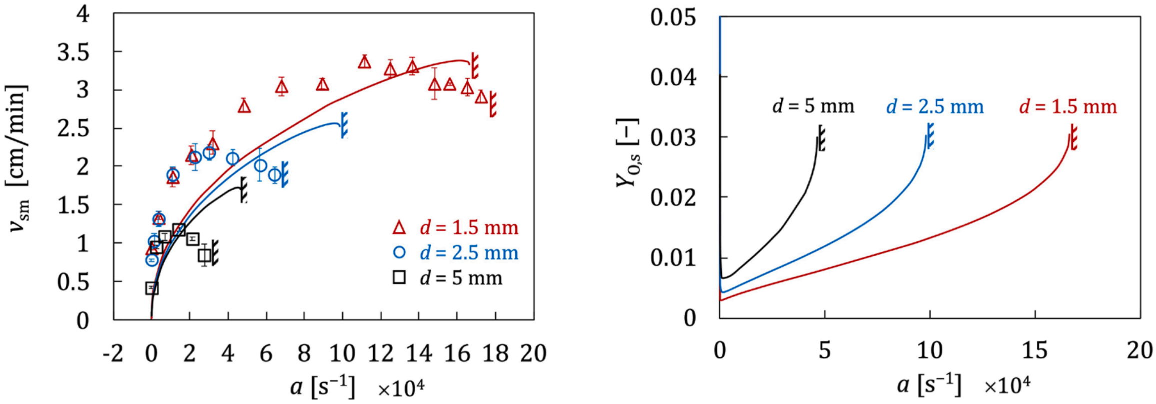

(a) (b)

Fig. 5. (a) smoldering rate, v_{sm}, (b) oxygen mass fraction at the surface, $Y_{O,s}$, as a function of strain rate a. Solid lines: calculation results; Open symbols: experimental data [1]; Red, blue, and black: $d = 1.5$, 2.5, and 5 mm.

2.5 mm and $d = 5$ mm. Future research should consider adding the differential terms in the radial direction to enhance the model's accuracy.

The surface oxygen mass fraction is an indicator of the intensity of the oxidation reaction. Fig. 5(b) shows an increase in the surface oxygen mass fraction, $Y_{O,s}$, near each limit condition, where the reaction is weak and oxygen is not fully consumed. It is also found that $Y_{O,s}$ increases with increasing d. Interestingly, the critical $Y_{O,s}$ near the blowoff limit is around 0.028 for all diameters.

3.4. *Extinction mechanisms*

Fig. 6(a) and (b) show the predicted smoldering rate and surface temperature as a function of strain rate, respectively. Without radiative heat loss, the surface temperature is predicted to be much higher at the low strain rates, as indicated by the dotted line, showing the significant role of radiative heat loss in smothering extinction. On the other hand, convective heat loss becomes more crucial at a higher strain rate near the blowoff limit, as confirmed by the difference between the dashed and dotted lines. Without the convective heat loss caused by the forced airflow, radiative heat loss is insufficient to blow off the reaction; the blowoff limit is overestimated at an extremely high strain rate with $h = 0$. The results align more closely with the experimental data (Fig. 5(a)) when accounting for both heat loss mechanisms, as shown by the solid lines. Thus, considering both heat loss mechanisms is crucial in predicting blowoff and smothering conditions.

3.5. *Limiting oxygen concentration (LOC)*

Fig. 7(a) summarizes the minimum oxygen concentration required to sustain the smoldering propagation at various fuel diameters. The graph illustrates a broad smoldering boundary compared to the flaming spread [7]. The extinction boundary consists of a smothering branch in the low airflow velocity region and a blowoff branch in the high airflow velocity region. The smothering and blowoff branches merge smoothly at the bottom, indicating the limiting oxygen concentration (LOC) below which smoldering propagation will not occur for any flow velocities.

The effect of fuel diameter on LOC is also examined, revealing an increasing LOC value with the diameter. A larger diameter of 5 mm shows a higher LOC of around 16%. The airflow velocity at LOC also

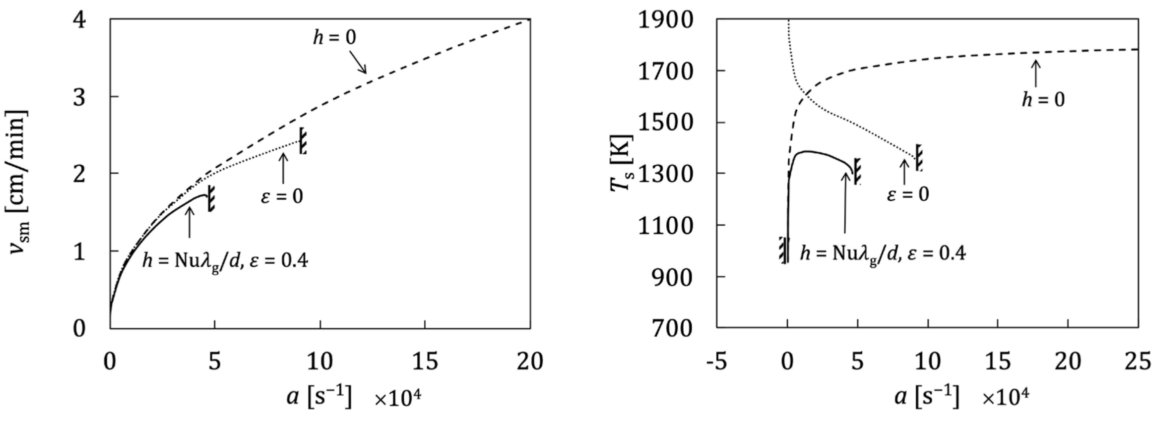

(a) (b)

Fig. 6. Effect of heat losses on predicted (a) smoldering rate, v_{sm}, (b) surface temperature, T_s, as a function of strain rate a for $d = 5$ mm. Dashed lines: $h = 0$, $\varepsilon = 0.4$; Dotted lines: $h = \mathrm{Nu}\lambda_g/d$, $\varepsilon = 0$; Solid lines: $h = \mathrm{Nu}\lambda_g/d$, $\varepsilon = 0.4$.

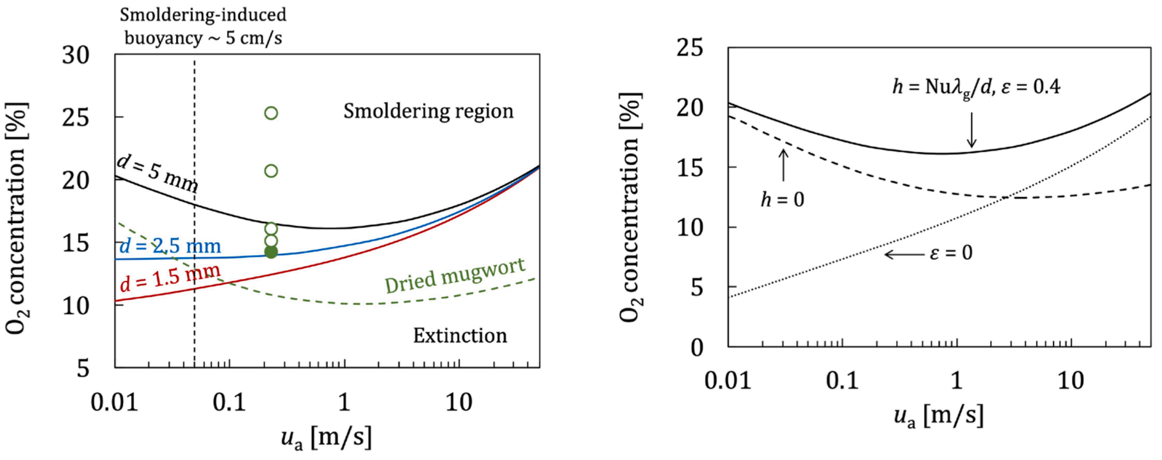

(a) (b)

Fig. 7. Predicted limit condition as a function of forced airflow velocity, u_a: (a) effect of diameter, (b) effects of heat loss mechanisms for $d = 5$ mm. Green symbol and line: measured [16] and predicted data of dried mugwort for $d = 18$ mm. ○: Combustible; ●: Extinction.

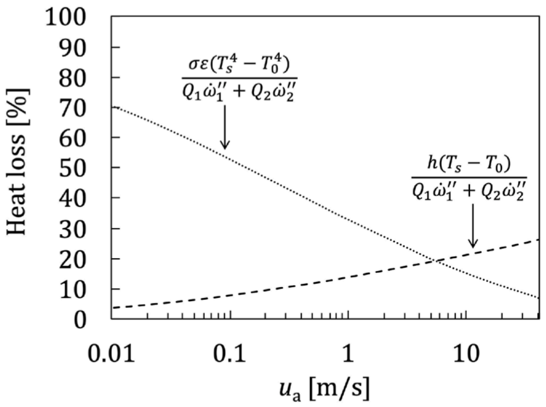

Fig. 8. Heat loss percentage as a function of airflow velocities, u_a, for $d = 5$ mm and $Y_{O,0} = 0.23$.

increases with d. These results contradict the previous discussion about the flaming spread on solid fuels [23], an interesting difference between smoldering and flaming spread.

The typical flammability map presented in [8] emphasizes the importance of fire safety in spacecraft due to a lower LOC in microgravity environments. For flaming spread, typical natural convection velocities are higher than the critical airflow velocity at LOC. Therefore, in normal gravity, natural convection leads to blowoff extinction at an oxygen concentration higher than LOC, resulting in a higher apparent LOC than microgravity. The situation is similar in the smoldering spread for $d = 1.5$ and 2.5 mm, where the natural convection velocity (around 5 cm/s [24]) is higher than the critical airflow velocity at LOC. On the other hand, for $d = 5$ mm, smoldering is possible at oxygen concentrations as low as LOC, even in normal gravity.

The experimental data of the extinction limit of dried mugwort from [16] are plotted as a green symbol in Fig. 7(a) and compared with the present model. Ref. [16] varied the oxygen concentration at a constant forced airflow to observe the extinction, shown as the filled symbol (●). Since the material properties of the dried mugwort are different from those of incense sticks, the values of $B_2 = 1 \times 10^5$ m^4/kg s and $\rho_F\phi_F = 440$ kg/m^3 are used, following [16]. The predicted result, represented by the green dashed line, shows that the model underestimates the extinction limit. Nevertheless, the limited available experimental data makes it difficult to draw definitive conclusions, highlighting the need for further validation with additional experimental data for the present configuration. Specifically, experiments that explore the extinction limit under low oxygen concentrations would help improve the model.

Fig. 7(b) shows the limit conditions for $d = 5$ mm predicted by considering different heat loss mechanisms. When the convective heat loss is ignored ($h = 0$), the blowoff limit at high airflow velocities is not accurately predicted. In contrast, the smothering limit at low airflow velocities cannot be predicted when the radiative heat loss is ignored ($\varepsilon = 0$), aligning with the results shown in Fig. 6. Fig. 8 shows the ratios of radiative and convective heat loss to the total reaction heat as functions of airflow velocity. The predominant heat loss mechanism is radiation at low airflow velocities. The intersection point at around 5 m/s signifies the transition into an apparent convective role.

4. Conclusions

A reduced model for smoldering propagation under a concurrent airflow is developed. The governing equations are derived by considering one-dimensional mass, energy, and oxygen balance. Five unknown parameters, i.e., $u_{g,s}$, T_p, T_s, v_{sm}, and $Y_{O,s}$, are solved simultaneously as part of the solutions. Despite the model's simplicity, the predicted results qualitatively agree with the previous experiment [1].

The model correctly reproduces experimental trends: the smoldering rate decreases with an increase in fuel diameter, and blowoff occurs at a lower airflow velocity for a thicker fuel. The significant role of convective heat loss at a high airflow regime is confirmed by investigating the effects of various modes of heat loss on extinction. Excluding the convective heat loss term, the blowoff extinction by the airflow cannot be predicted within a reasonable range of airflow velocity. On the other hand, the smothering branch at low airflow velocities cannot be predicted without considering the heat loss by radiation. The effect of oxygen concentration is investigated based on the constructed LOC curve. The results show the increasing LOC with an increasing fuel diameter. The influence of gravity level on LOC for the smoldering spread is also discussed.

CRediT authorship contribution statement

Pichayaporn Viriya-amornkij: Writing – original draft, Methodology, Investigation, Formal analysis. **Kazunori Kuwana:** Writing – review & editing, Supervision, Project administration, Funding acquisition, Conceptualization. **Xinyan Huang:** Writing – review & editing, Validation, Investigation.

Declaration of competing interest

The authors declare that they have no known competing financial interests or personal relationships that could have appeared to influence the work reported in this paper.

Acknowledgment

A part of this work was supported by JSPS KAKENHI Grant Number JP21H04593.

Appendix A

The sensitivity analysis of model parameters, such as B_2, ε, and E_2, is conducted as shown in Figs. A1 and A2, respectively. Figs. A1(a) and (b) show the smoldering rate predicted using B_2 and ε with ±5% perturbation. The results show that changes in B_2 and ε influence only the extinction limit, not the smoldering rate itself. The effect of B_2 and ε on the blowoff strain rate is tested for all diameters within ± 25% perturbation of its original values, as shown in Figs. A1(c) and (d), representing the increasing blowoff strain rate with increasing B_2 and decreasing ε.

The sensitivity of E_2 is analyzed with ± 5% perturbation of its original value, as shown in Fig. A2. Note that for each perturbation, assigning a value of E_2 necessitates adjusting B_2 to align with the experimental data. Fig. A2 shows that the choice of E_2 does not impact the results.

Appendix B

The effect of Nu correlations is evaluated through a comparison between the correlations for spheres (applied in this study) and those for falling liquid drops [25]: $\mathrm{Nu} = 2 + 0.6\mathrm{Re}^{1/2}\mathrm{Pr}^{1/3}$. The calculation is conducted using all the same model's settings, except for the Nu correlations. Fig. B1 shows the predicted smoldering rates using the Nu correlations for falling liquid drops, indicating a significant deviation from the experimental data, especially for $d = 2.5$ mm and 5 mm, when compared to Fig. 5(a). While the combination of Nu/Sh correlations applied in this study allows the reproduction of similar trends with the experimental data, there is room to improve the model's accuracy through the careful selection of Nu/Sh correlations.

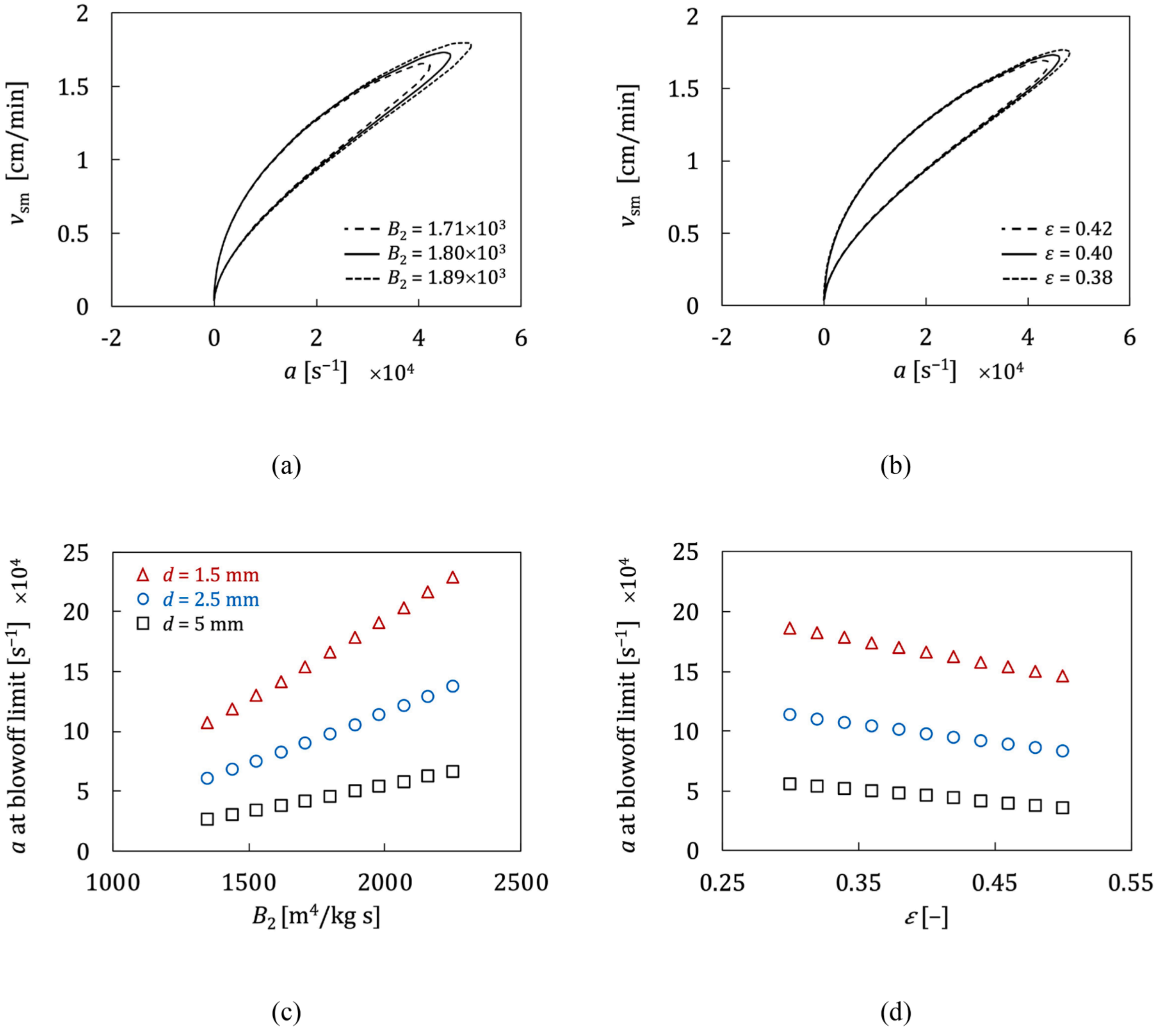

Fig. A1. Model parameters sensitivities (a) B_2 with ±5% perturbation, (b) ε with ±5% perturbation for $d = 5$ mm, (c) effect of B_2 on blowoff strain rate with ±25% perturbation, and (d) effect of ε on blowoff strain rate with ±25% perturbation.

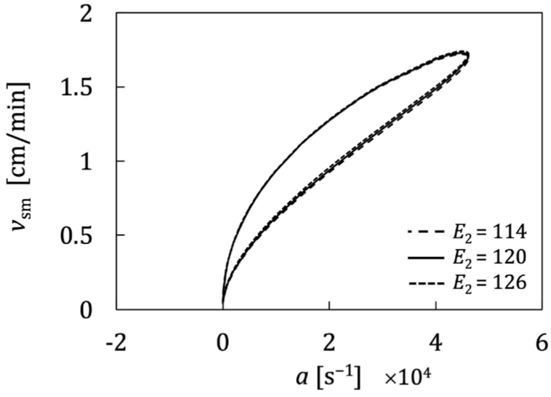

Fig. A2. Model parameters sensitivities E_2 with ±5% perturbation for $d = 5$ mm.

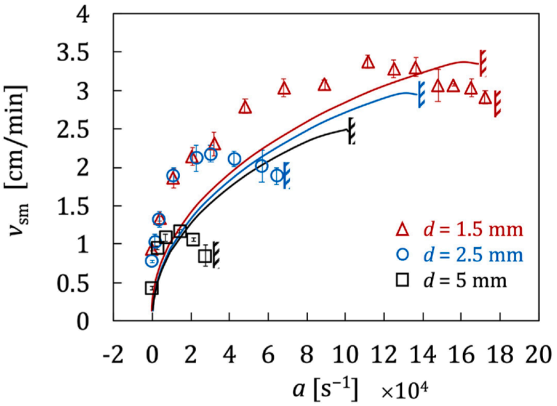

Fig. B1. Predicted smoldering rate, v_{sm}, and extinction limits based on $\mathrm{Nu} = 2 + 0.6\mathrm{Re}^{1/2}\mathrm{Pr}^{1/3}$. Solid lines: calculation results; Open symbols: experimental data [1]; Red, blue, and black: $d = 1.5$, 2.5, and 5 mm.

References

[1] S. Lin, T.H. Chow, X. Huang, Smoldering propagation and blow-off on consolidated fuel under external airflow, Combust. Flame 234 (2021) 111685.

[2] A.C. Fernandez-Pello, S.R. Ray, I. Glassman, Flame spread in an opposed forced flow: the effect of ambient oxygen concentration, Symp. Combust. Proc. 18 (1981) 579–589.

[3] K.N. Palmer, Smouldering combustion in dusts and fibrous materials, Combust. Flame 1 (1957) 129–154.

[4] A.F. Osorio, C. Fernandez-Pello, D.L. Urban, G.A. Ruff, Limiting conditions for flame spread in fire resistant fabrics, Proc. Combust. Inst. 34 (2013) 2691–2697.

[5] L. Yermán, H. Wall, J.L. Torero, Experimental investigation on the destruction rates of organic waste with high moisture content by means of self-sustained smoldering combustion, Proc. Combust. Inst. 36 (2017) 4419–4426.

[6] S. Lin, X. Huang, Quenching of smoldering: effect of wall cooling on extinction, Proc. Combust. Inst. 38 (2021) 5015–5022.

[7] S.L. Olson, P.V. Ferkul, J.S. T'ien, Near-limit flame spread over a thin solid fuel in microgravity, Symp. Combust. Proc. 22 (1989) 1213–1222.

[8] S. Takahashi, M.A.F. bin Borhan, K. Terashima, A. Hosogai, Y. Kobayashi, Flammability limit of thin flame retardant materials in microgravity environments, Proc. Combust. Inst. 37 (2019) 4257–4265.

[9] S. Bhattacharjee, W. Tran, M. Laue, C. Paolini, Y. Nakamura, Experimental validation of a correlation capturing the boundary layer effect on spread rate in the kinetic regime of opposed-flow flame spread, Proc. Combust. Inst. 35 (2015) 2631–2638.

[10] S. Bhattacharjee, A. Simsek, S. Olson, P. Ferkul, The critical flow velocity for radiative extinction in opposed-flow flame spread in a microgravity environment: a comparison of experimental, computational, and theoretical results, Combust. Flame 163 (2016) 472–477.

[11] Y. Qin, Y. Chen, S. Lin, X. Huang, Limiting oxygen concentration and supply rate of smoldering propagation, Combust. Flame 245 (2022) 112380.

[12] M.K. Moallemi, H. Zhang, S. Kumar, Numerical modeling of two-dimensional smoldering processes, Combust. Flame 95 (1993) 170–182.

[13] F. Richter, F.X. Jervis, X. Huang, G. Rein, Effect of oxygen on the burning rate of wood, Combust. Flame 234 (2021) 111591.

[14] S. Takahashi, H. Ito, Y. Nakamura, O. Fujita, Extinction limits of spreading flames over wires in microgravity, Combust. Flame 160 (2013) 1900–1902.

[15] S. Bhattacharjee, T. Delzeit, Opposed-flow flame spread over cylindrical fuels: spread rate formulas and experimental verification, Proc. Combust. Inst. 39 (2023) 3863–3870.

[16] O. Kadowaki, M. Suzuki, K. Kuwana, Y. Nakamura, G. Kushida, Limit conditions of smoldering spread in counterflow configuration: extinction and smoldering-to-flaming transition, Proc. Combust. Inst. 38 (2021) 5005–5013.

[17] H. Tsuji, Counterflow diffusion flames, Prog. Energy Combust. Sci. 8 (1982) 93–119.

[18] W.H. McAdams, Heat Transmission, McGraw-Hill, New York, U.S., 1954, p. 266.

[19] P.L.T. Brian, H.B. Hales, Effects of transpiration and changing diameter on heat and mass transfer to spheres, AIChE J. 15 (1969) 419–425.

[20] T. Kashiwagi, H. Nambu, Global kinetic constants for thermal oxidative degradation of a cellulosic paper, Combust. Flame 88 (1992) 345–368.

[21] M. Gupta, J. Yang, C. Roy, Specific heat and thermal conductivity of softwood bark and softwood char particles, Fuel 82 (2003) 919–927.

[22] S.Z. Miry, M.A.B. Zanoni, T.L. Rashwan, J.L. Torero, J.I. Gerhard, Investigation of multi-dimensional transfer effects in applied smouldering systems: a 2D numerical modelling approach, Combust. Flame 246 (2022) 112385.

[23] A.S. Rangwala, S.G. Buckley, J.L. Torero, Upward flame spread on a vertically oriented fuel surface: the effect of finite width, Proc. Combust. Inst. 31 (2007) 2607–2615.

[24] M. Goto, K. Kuwana, G. Kushida, S. Yazaki, Experimental and theoretical study on near-floor flame spread along a thin solid, Proc. Combust. Inst. 37 (2019) 3783–3791.

[25] W.E. Ranz, W.R. Marshall, Evaporation from drops, Chem. Eng. Prog. 48 (1952) 141–146.